1   *Article*

2   # Neuronal Lipoprotein Lipase Deficiency alters
3   # Neuronal Function and Hepatic Metabolism

4   **Kimberley D. Bruce[1]*, Evgenia Dobrinskikh[2], Hong Wang[1], Ivan Rudenko[1], Hong Gao[3], Andrew**
5   **E. Libby[4], Sachi Gorkhali[1], Tian Yu[1], Andrea Zsombok[3], Robert H. Eckel[1]**

6   [1] Division of Endocrinology, Metabolism, & Diabetes, University of Colorado Denver Anschutz Medical
7   Campus, Aurora, Colorado
8   [2] Department of Medicine, University of Colorado Denver Anschutz Medical Campus, Aurora, Colorado
9   [3] Department of Physiology, School of Medicine, Tulane University, New Orleans, Louisiana
10 [4] Department of Biochemistry and Molecular & Cellular Biology, Georgetown University Medical Center,
11   Washington, DC
12
13
14 * Correspondence: kimberley.bruce@cuanschutz.edu

15 **Abstract:** The autonomic regulation of hepatic metabolism offers a novel target for the treatment of
16 non-alcoholic fatty liver disease (NAFLD). However, the molecular characteristics of neurons that
17 regulate the brain-liver axis remain unclear. Since mice lacking neuronal lipoprotein lipase (LPL)
18 develop perturbations in neuronal lipid-sensing and systemic energy balance, we reasoned that LPL
19 might be a component of pre-autonomic neurons involved in the regulation of hepatic metabolism.
20 Here we show that despite obesity, mice with reduced neuronal LPL (NEXCreLPLflox [LPL KD])
21 show improved glucose tolerance and reduced hepatic lipid accumulation with aging compared to
22 WT controls (LPLflox). To determine the effect of LPL deficiency on neuronal physiology, liver-
23 related neurons were identified in the paraventricular nucleus (PVN) of the hypothalamus using
24 the transsynaptic retrograde tracer PRV-152. Patch-clamp studies revealed reduced inhibitory post-
25 synaptic currents in liver-related neurons of LPL KD mice. Fluorescence Lifetime Imaging
26 Microscopy (FLIM) was used to visualize metabolic changes in LPL-depleted neurons.
27 Quantification of the free vs. bound Nicotinamide Adenine Dinucleotide (NADH) and Flavin
28 Adenine Dinucleotide (FAD) revealed increased glucose utilization and TCA cycle flux in LPL-
29 depleted neurons compared to controls. Global metabolomics from hypothalamic cell lines either
30 deficient in, or over-expressing, LPL recapitulated these findings. Our data suggest that LPL is a
31 novel feature of liver-related preautonomic neurons in the PVN. Moreover, LPL loss is sufficient to
32 cause changes in neuronal substrate utilization and function, which may precede changes in hepatic
33 metabolism.

34 **Keywords:** lipoprotein lipase; neuronal metabolism; fatty liver; brain-liver-axis; FLIM
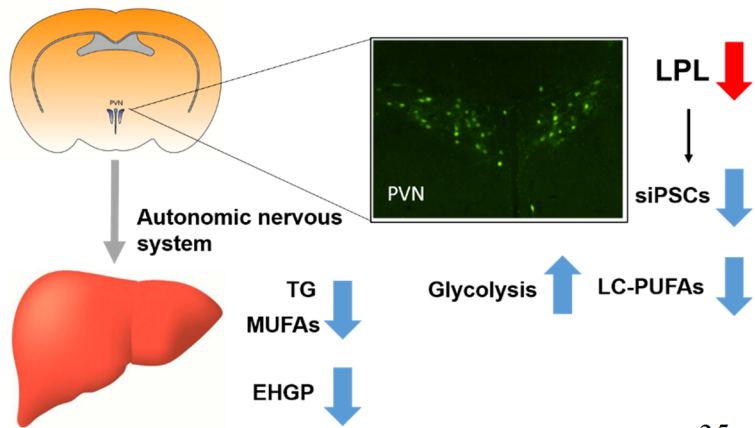
Graphical Abstract. Reduced neuronal LPL is associated with altered neuronal activity and metabolism, and hepatic lipid and glucose homeostasis.

35

1. Introduction

The liver is central to the pathogenesis of metabolic disorders such as obesity, type 2 diabetes mellitus (T2DM), and cardiovascular disease. It is thought that hepatic lipid accumulation precedes insulin resistance [1, 2], which plays a pivotal role in the development of T2DM [3]. Importantly, hepatic neutral lipid accumulation and the incidence of non-alcoholic fatty liver disease (NAFLD) increase markedly with age [4]. Thus, preventing hepatic fat accumulation is a promising strategy to prevent age-associated metabolic disease. The autonomic nervous system (ANS) plays a key role in regulating hepatic metabolism [5] and is, therefore, an attractive target for the treatment of metabolic disease. Metabolic signals from the hypothalamus reach the liver via neuronal pathways that include the brain stem, sympathetic nerves, and the vagus nerve. However, the metabolic characteristics of hypothalamic preautonomic neurons remain undefined.

The accumulation of intermediary metabolites in specific brain regions can alter hepatic metabolism, suggesting that the brain-liver axis is involved in responding to nutrient status and maintaining whole-body energy homeostasis. For example, central administration of glucose stimulates the conversion of lactate to pyruvate and activates a K_{ATP} channel-dependent pathway within the hypothalamus, leading to lowered VLDL-TG secretion from the liver and reduced circulating triglycerides (TG) [6]. In addition, fatty acids (FA) such as oleic acid activate a PKC-δ - K_{ATP} channel signaling pathway, resulting in suppressed VLDL-TG secretion in rats [7]. This signaling requires the dorsal vagal complex, highlighting a brain-liver neurocircuitry in which hypothalamic FA-sensing triggers a hepatic-neuronal relay to regulate hepatic lipid homeostasis [7]. However, the precise cellular components involved in neuronal FA sensing remain unclear. While several FA transporters have been identified in the brain, these are only associated with specific FA species and do not account for the unique composition of lipid substrates in the brain, i.e., glial-derived lipoproteins. For example, CD36 knock-out mice show reduced monounsaturated FA incorporation into brain phospholipids, but no changes in essential polyunsaturated fatty acids (PUFA) concentration [8], suggesting that alternative pathways may regulate PUFA uptake and metabolism.

We and others have previously shown that lipoprotein lipase (LPL)—the rate-limiting enzyme in the hydrolysis of TG-rich lipoproteins and FA uptake—is involved in neuronal lipid uptake and the co-ordination of systemic metabolism [9-13]. Specifically, mice with neuronal LPL deficiency develop obesity by six months of age and a specific PUFA deficiency associated with neurobehavioral abnormalities [11, 13]. Thus, based on the systemic impact of neuronal LPL deficiency, we reasoned that neuronal LPL may play a role in hypothalamic lipid-sensing and the ANS regulation of hepatic metabolism. In the present study, we demonstrate that obese mice with neuronal LPL deficiency show improved glucose tolerance with aging, involving reduced hepatic lipid accumulation and altered activity of liver-related neurons in the PVN. Moreover, LPL depletion is sufficient to alter neuronal substrate metabolism *in vitro* and *in vivo*, suggesting that LPL-dependent changes to neuronal metabolic flux may precede changes in systemic metabolism

2. Results

2.1. Mice with neuron-specific LPL depletion have improved glucose tolerance

To determine whether neuronal LPL deficiency could influence peripheral glucose homeostasis, we performed 2-hour intraperitoneal (IP) glucose tolerance tests (GTT) in LPL KD (NEXCreLPL[flox]) and WT (LPL[flox]) mice at 3, 6, 12, and 18 months of age (Fig. 1A-D). LPL KD mice showed improved glucose clearance by 6 mo., with lower plasma glucose concentrations throughout the study ($P<0.05$ versus WT) (Fig. 1B). LPL KD mice showed lower plasma glucose concentrations at 12 and 18 mo.,

82   compared to WT mice (Fig. 1C-D). Importantly, LPL KD mice were markedly heavier than controls
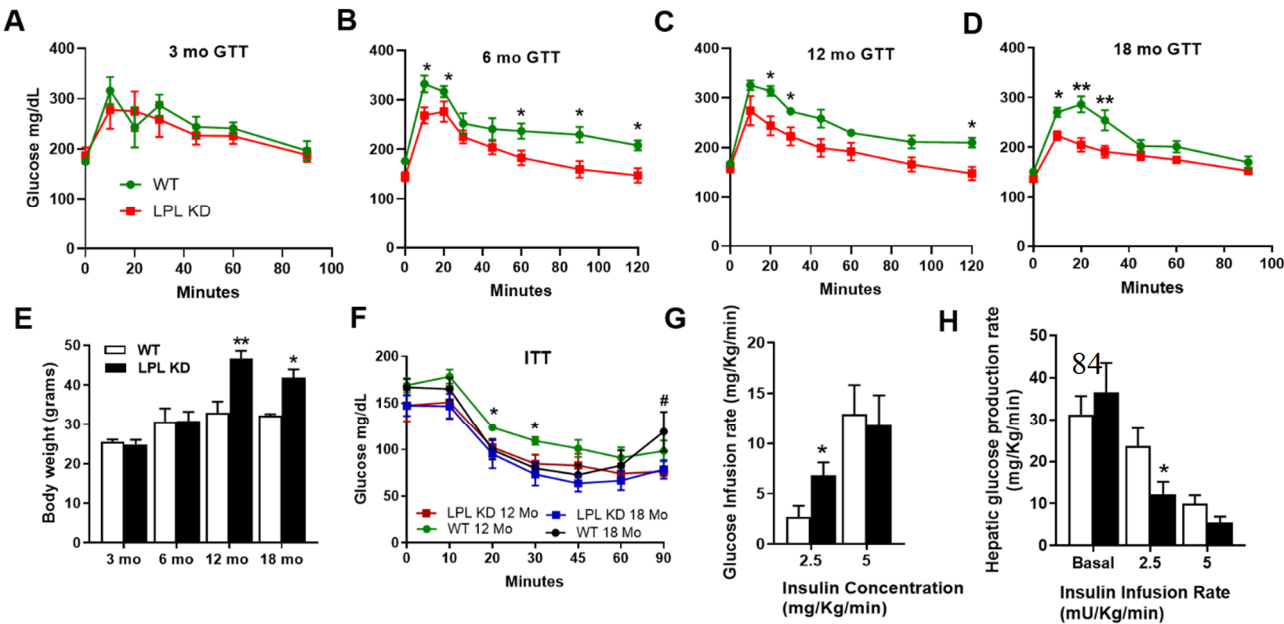83   by 12 mo. (Fig.1E).

Figure 1. Neuronal LPL deficiency improves glucose tolerance with aging. A-D. Measurements of glucose tolerance in (NEXCreLPL^{flox}) LPL KD versus WT (LPL^{flox}) mice at 3 **(A),** 6 **(B),** 12 **(C)** and 18 **(D)** mo. **E.** The body weights of LPL KD (black) and WT (white) mice before terminal experiments at each age point. **F**. IP insulin tolerance tests (ITT) in 12 and 18 mo in WT mice. **G**. Steady state whole body glucose infusion rate in LPL KD (black) mice compared to WT (white). **H**. Endogenous glucose production (EGP) rate in LPL KD mice compared to WT controls. (Where # = P<0.1, * = P<0.05, and ** = P<0.01 vs aged-matched WT controls).

85   *3.2. LPL KD mice have reduced hepatic glucose production*

86   Since neuronal LPL deficiency is associated with improved glucose tolerance despite obesity, we
87   reasoned that these animals may be more insulin sensitive. To test this, mice were given an IP bolus
88   of insulin at 12 and 18 mo. Although both WT and LPL KD mice responded to the insulin bolus, this
89   response was greater in the 12 mo. LPL KD mice compared to WT (P<0.05 at 20 and 30 minutes), and
90   longer-lasting in the 18 mo. LPL KD mice, with a trend for plasma glucose levels rising more rapidly
91   in the WT controls (P<0.09) (Fig 1F).
92
93   In patients with T2DM, endogenous glucose production (EGP) is the primary factor responsible
94   for elevations in fasting plasma glucose levels and contributes importantly to postprandial
95   hyperglycemia. Thus, we hypothesized that the age-associated improvements in glucose tolerance
96   observed in the LPL KD mice may be due to lower EGP. Hence, we performed hyperinsulinemic-
97   euglycemic clamps to show that hepatic, but not systemic insulin sensitivity, was increased in LPL
98   KD mice compared to WT mice, an effect demonstrated at low physiological insulin infusion rates
99   [14], i.e., 2.5 mg/kg/min (Fig. 1G). In addition, LPL KD mice showed an increased ability of insulin to
100   suppress EGP at low insulin concentrations (Fig. 1H).
101

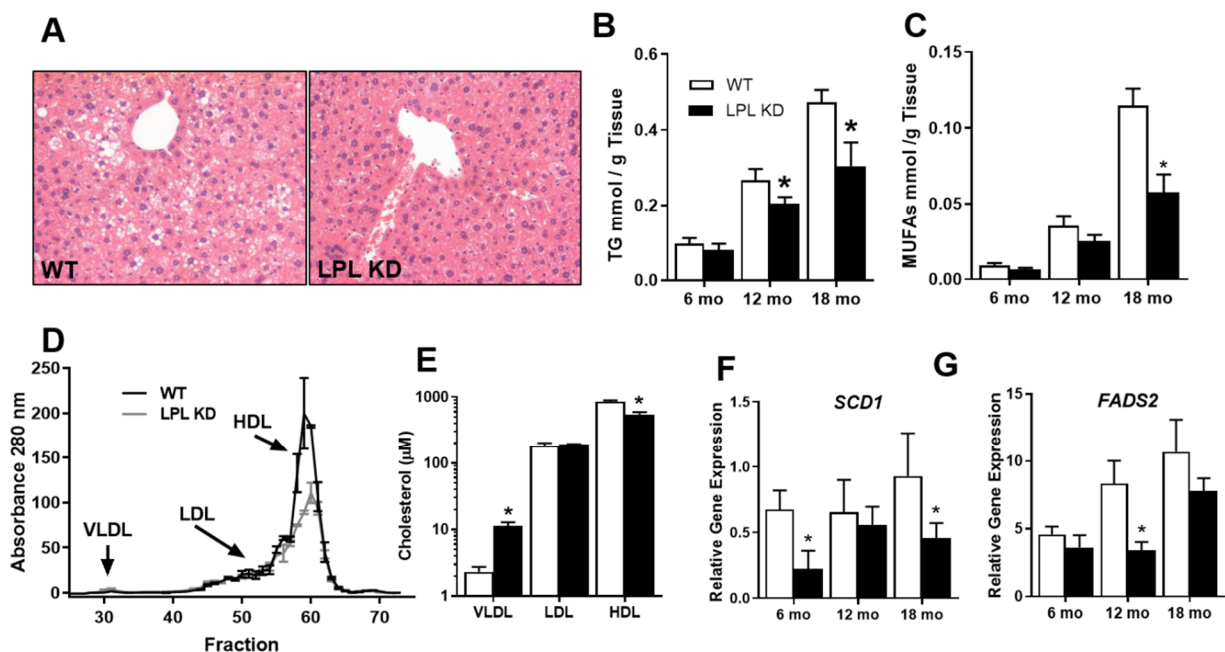102   *3.3. Neuronal LPL-KD mice have reduced hepatic lipid accumulation*

Figure 2. Hepatic lipid accumulation is reduced in neuron-specific LPL KD mice. A. H and E stained liver of 12 mo. WT (LPLflox) and LPL KD (NEXCreLPLflox) mice. **B**. Hepatic triglyceride (TG) concentration in LPL KD (black bars) compared to WT mice (white bars) at 6, 12 and 18 mo. **C**. Hepatic mono-unsaturated fatty acid (MUFA) concentration reduced in LPL KD mice compared to WT mice at 6, 12 and 18 mo**. D.** FPLC fractionation of lipoproteins from plasma of LPL KD and WT mice at 18 mo. **E**. Cholesterol content of lipoprotein fractions at 18 mo. **F-G**. Relative gene expression of *SCD1* and *FADS2* at 6, 12 and 18 mo. (* = P<0.05 vs aged-matched WT controls).

103   Since hepatic lipid accumulation can precede changes in hepatic insulin sensitivity [15], we
104   hypothesized that changes in glucose tolerance and insulin sensitivity in the LPL KD mice were a
105   consequence of altered hepatic lipid metabolism. Thus, we performed histological analysis to
106   determine hepatic steatosis in the livers of 12 mo. WT and LPL KD mice. Lipid droplets were clearly
107   visible in liver sections from WT mice and were present as moderate micro-vesicular steatosis (Fig.
108   2A). However, fewer lipid droplets were observed in liver sections from the LPL KD mice (Fig. 2A).
109   We also observed a reduced total TG content in the livers of LPL KD mice at 12 and 18 mo. (Fig 2B).
110   In fact, this decrease was observed in almost all lipid species (data not shown), with the greatest
111   difference being observed in the monounsaturated (MUFA) content at 18 mo. (Fig. 2C).
112
113   Since VLDL export from the liver is a major contributor towards hepatic lipid homeostasis [16],
114   we measured the plasma lipoprotein profile of LPL KD and WT mice at 18 mo. (Fig. 2D). Importantly,
115   as samples are separated by size exclusion chromatography absorbance is measured at 280 nm.
116   Therefore, the trace shown indicates the protein concentration of the eluted sample, and allows
117   identification of the lipoprotein fractions (Fig. 2D). Cholesterol was then subsequently measured for
118   each lipoprotein class. We observed an increase in plasma VLDL-cholesterol concentrations in LPL
119   KD vs WT mice (P<0.05 vs WT) (Fig. 2E). Of note, low density lipoprotein (LDL) cholesterol
120   concentrations were almost identical between the LPL KD and WT mice. However, plasma high-
121   density lipoprotein (HDL) cholesterol was lower in the LPL KD mice (P<0.05 vs WT) (Fig. 2E).
122
123   To further understand the mechanism behind altered lipid metabolism in the livers of mice
124   lacking neuronal LPL, we measured the expression of genes key to hepatic lipid homeostasis.
125   Stearoyl-CoA desaturase (SCD1), the rate-limiting enzyme in MUFA synthesis was reduced in the
126   LPL KD mice at 6 and 18 mo. (Fig. 2F). In addition, fatty acid desaturase 2 (FADS2), which catalyzes
127   the first and rate-limiting step in several fatty acid desaturation pathways showed a robust increase
128   with age (Fig 2G), which was blunted in the LPL KD mice at 12 mo. (P<0.05 vs. WT) (Fig 2G).

129
130   *3.4. Liver-related PVN neurons of LPL KD mice have reduced inhibitory synaptic control*
131   A growing number of studies suggest that the activity of preautonomic neurons in the PVN of
132   the hypothalamus has a pivotal role in the autonomic regulation of hepatic glucose and lipid
133   metabolism *[17-20]*. Since synaptic inputs largely contribute to the excitability of neurons, we
134   reasoned that the synaptic control of liver-related neurons in the PVN is altered in mice with neuronal
135   LPL deficiency. Liver-related PVN neurons were identified with the retrograde transsynaptic viral
136   tracer PRV-152 (Fig. 3A), and inhibitory and excitatory post-synaptic currents were recorded from
137   EGFP expressing PVN neurons. The observed EGFP labeling indicated liver-related preautonomic
138   neurons in the PVN (Fig. 3B), consistent with previous findings *[17]*. Our data showed decreased
139   inhibitory post-synaptic currents (IPSC) frequency in LPL KD mice compared with WT mice (Fig.
140   3C). The average frequency of spontaneous inhibitory post-synaptic currents (sIPSCs) was 0.97 ± 0.07
141   Hz in LPL KD mice, while 3.56 ± 0.93 Hz in WT mice suggesting that inhibitory neurotransmission to
142   liver-related PVN neurons is reduced in LPL KD mice ($P < 0.05$) (Fig. 3D). In contrast, we did not find
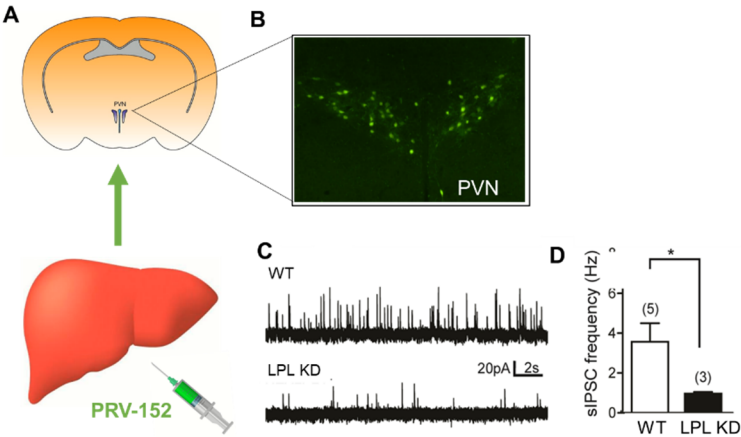

Figure 3. Decreased inhibitory synaptic regulation of liver related PVN neurons in LPL KD mice. A-B. Liver-related neurons in the PVN were identified with a retrograde transsynaptic viral tracer (PRV-152), and used for patch-clamp recordings. **C**. Recordings of sIPSCs in WT (LPL^{flox}) and LPL KD (NEXCreLPL^{flox}) mice. **D**. The frequency of sIPSCs was reduced in LPL KD mice compared to WT mice. (* = $P < 0.05$ vs WT).

143   significant differences in excitatory neurotransmission
144   ($P > 0.05$).
145
146
147   *3.5. Loss of LPL in PVN neurons alters metabolic flux*
148
149   We have previously shown that neuronal LPL plays an important role in neuronal lipid sensing.
150   However, the mechanism underlying this process remains unknown. Since the canonical role of LPL
151   is to facilitate cellular lipid uptake, we hypothesized that LPL loss might alter neuronal metabolism.
152   A major limiting factor regarding metabolic studies in neurons is the ability to preserve endogenous
153   metabolism at the time of quantification, without causing major changes during ex-vivo culture.
154   Indeed, many primary cultures of neurons are from the early post-natal period, and endogenous
155   metabolism may differ vastly from that in the adult mouse. Here, we employed Fluorescence Lifetime
156   Imaging Microscopy (FLIM) as a novel method to measure the endogenous metabolic status of
157   neurons from fresh-frozen brain tissue with high spatial resolution. LPL was depleted in neurons of
158   the PVN in LPL$^{flox/flox}$ mice using adenoviral delivery of a GFP-Cre virus, driven by the neuronal-
159   specific CamKIIα promoter (Fig. 4A). GFP allowed for localization to the PVN (Fig. 4A), and to
160   neurons (Fig. 4B), which is essential since it is not yet studied how fixation and/or staining alters the
161   ability to measure and discriminate between the lifetimes of NADH and FAD co-enzymes. Overall,
162   we showed that there was a significant shift towards free versus bound NADH in LPL deficient PVN
163   neurons ($P < 0.05$) (Fig. 4D), which indicates increased flux through metabolic pathways producing
164   free NADH (e.g., glycolysis), rather than flux through metabolic pathways in which NADH would
165   be bound to metabolic enzymes (i.e., oxidative phosphorylation). Moreover, there was a dramatic
166   shift in the proportion of free FAD versus bound FAD ($P < 0.001$) (Fig. 4E), which suggests an increase
167   in processes that produce free FAD (e.g., TCA), and a reduction in process in which enzymes utilize
168   FAD as a cofactor (e.g., oxidative phosphorylation and FA oxidation).
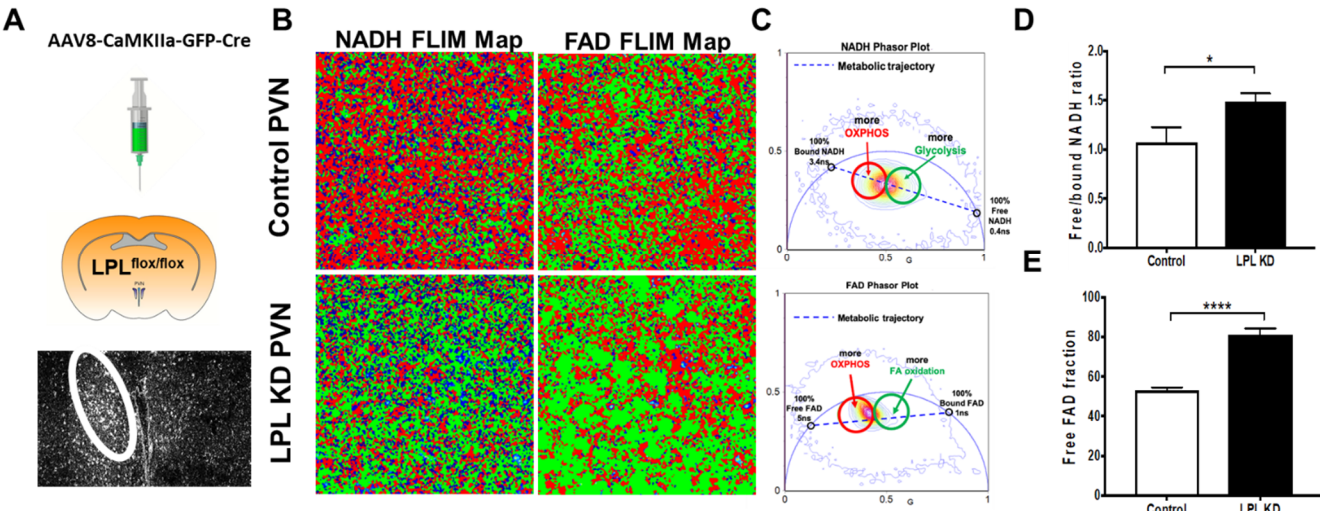
169

Figure 4. LPL depletion in neurons of the paraventricular nucleus of the hypothalamus (PVN) results in altered neuronal metabolism. A. LPL was depleted in the PVN of LPL^{flox} mice by the delivery of AAV8-CaMKIIa-GFP-Cre, whereas AAV8-CaMKIIa-GFP was administered to control mice. **B.** Representative images of NADH and FAD FLIM Maps from images of the PVN in Control versus LPL KD Mice. **C.** Phasor plots, showing the shift in metabolic trajectory with changing lifetime for NADH and FAD. **D.** Increased ratio of free/bound NADH in LPL KD PVN neurons. **E.** Increased free FAD fraction in LPL KD PVN neurons. (* = P<0.05 vs WT, ****= P<0.0001 vs WT)

170
171   To validate changes in substrate utilization following LPL loss, we measured global metabolites
172   in hypothalamic neuronal cell lines in which LPL was either depleted (LPL KO N41) or over-
173   expressed (LPL OE N41). Although immortalized or primary cell lines cannot perfectly recapitulate
174   the in vivo studies described above, this established cell tool enables us to validate major changes in
175   metabolic pathways following LPL loss. Here, we found a marked increase in the abundance of
176   fructose 1-6-bisphosphate in LPL KO N41 neurons compared to control neurons (P<0.001) (Fig 5A
177   and Supplemental Figures). Although this suggests an increase in glucose utilization following LPL
178   loss via glycolysis, it also indicates increased carbohydrate metabolism; the pentose phosphate
179   pathway (PPP) being the preferred route of glucose utilization in neurons *[21]*. Importantly, increased
180   glucose utilization increases the production of free NADH, supporting the observation of increased
181   free NADH following LPL loss (Fig. 4D). In addition, we found an increase in the abundance of TCA
182   metabolites, such as citrate (P<0.05), malate (P<0.01), fumarate (P<0.001) and succinate (P<0.001) (Fig.
183   5B and Supplemental Fig 2) in LPL KO N41 neurons, suggesting an augmented flux through this
184   pathway and thus, increased free FAD production. Additional pathway analysis supported the over
185   representation of TCA metabolites in the LPL KD cells (Supplemental Figure 4). Interestingly, LC-
186   PUFAs were reduced in the LPL KO N41 neurons but increased in the LPL OE N41 neurons (Fig 5C
187   and Supplemental Fig 3). While this suggests that FA oxidation flux may be reduced, contributing to
188   free FAD accumulation, it also highlights LPL's selective role in the uptake of long-chain unsaturated
189   fatty acids, which is consistent with previous studies [10, 11, 13].
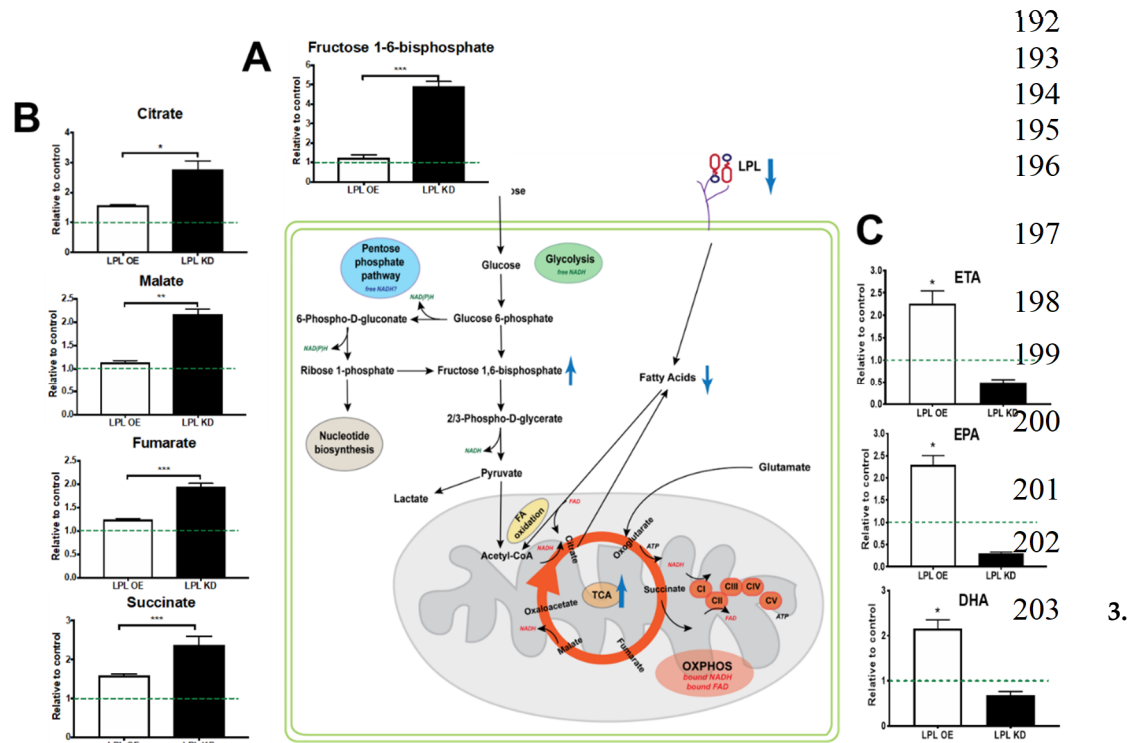190
191

Figure 5. Altered substrate utilization in hypothalamic neurons deficient in or over –expressing LPL. A. LPL KD N41 neurons show increased abundance of Fructose 1-6 bisphosphate. **B**. LPL KD N41 neurons show increased TCA intermediates. **C**. LPL OE N41 neurons have increased abundance of LC-PUFAs. * = P<0.05 vs WT, ** = P<0.01 vs WT, *** = P<0.001 vs WT.

Discussion

Since aberrant hepatic glucose production and lipid metabolism play a key role in the development of metabolic diseases such as IGT, T2DM, and even hypertriglyceridemia, identification of the mechanisms underlying the brain-liver axis holds promise for the development of novel interventions and therapeutics. Several studies have highlighted the ability of specific neuropeptides and metabolites to act upon key hypothalamic energy-sensing nuclei, and in turn, modulate downstream metabolism **[7, 22-24]**. However, how neurons receive such inputs is mostly unknown. The goal of the present study was to investigate whether LPL was involved in the regulation of hepatic metabolism by modulating neuronal metabolism. We reasoned that since mice with a neuron-specific LPL depletion show hyperphagia, inactivity, and obesity, autonomic regulation of the peripheral metabolic organs such as the liver was likely. Interestingly, we found that despite obesity, mice with reduced neuronal LPL showed improved glucose tolerance with aging, a phenotype that involves reduced hepatic EGP and preserved hepatic insulin sensitivity despite aging, and obesity.

Using GTTs in LPL KD and WT mice at several age points, we found that mice lacking neuronal LPL had improved glucose tolerance compared to WT controls, a key difference that became more pronounced with aging (Fig. 1). Importantly, by 12 mo., the LPL KD mice were heavier than WT mice. However, glucose tolerance was preserved throughout aging, despite obesity (Fig. 1). Although paradoxical, this phenotype is reminiscent of obese individuals who remain "metabolically healthy" **[25]**. These insulin-sensitive obese (ISO) individuals have lower visceral fat accumulation, less ectopic fat, and less systemic inflammation than insulin-resistant obese individuals **[26, 27]**. Interestingly, LPL KD mice exhibit brown adipose tissue hyperplasia [11], and reduced ectopic hepatic lipid accumulation (Fig 2A), both hallmarks of ISO. In further support, we show that LPL KD mice have improved hepatic insulin sensitivity (Fig. 2). Therefore, it is plausible that a reduction in neuronal LPL influences the autonomic regulation of systemic metabolism to mimic the ISO individuals.

229
230   The autonomic regulation of hepatic glucose metabolism is well established. Several studies
231 have demonstrated that stimulation of the splanchnic nerve (sympathetic nervous system [SNS])
232 modulates liver function, increases EGP, and decreases glycogenesis, whereas stimulating the vagus
233 nerve (parasympathetic nervous system [PNS]) decreases EGP and increases glycogenesis [28, 29].
234 Since we observed lower EGP in mice with reduced neuronal LPL, it is tempting to speculate that we
235 observe increased PNS activity in these animals compared to wild-type mice. However, we cannot
236 rule out the possibility that changes in EGP are due to reduced SNS activity. Thus, further studies are
237 needed to delineate this mechanism. Nonetheless, our findings support the notion that LPL is a
238 feature of preautonomic neurons involved in lipid sensing and the regulation of hepatic glucose
239 metabolism
240
241   The ANS is also involved in the regulation of hepatic lipid metabolism. Here we show that the
242 abundance of hepatic TG, MUFA (Fig. 2C), and the expression of *SCD1* (Fig. 2F) and *FADS2* (Fig. 2G)
243 increases robustly with age in WT mice. This increase in hepatic lipid species is reminiscent of the
244 increase in the prevalence of NAFLD in the aging population [4]. Since the SNS is dysregulated with
245 age [30] and has been implicated in the development of NAFLD [31], our data point to an age-
246 associated increase in SNS activity in WT mice. Importantly, mice with neuronal LPL deficiency have
247 reduced hepatic lipid accumulation, and lipogenic gene expression (Fig. 2) despite aging. Therefore,
248 it is tempting to speculate that the loss of neuronal LPL dampens an age-associated rise in SNS
249 activity with age. Since we observe a marked decrease in hepatic MUFA, and *SCD1*, the enzyme
250 responsible for the formation of mono-unsaturated acyl-CoAs from saturated acyl-CoAs, this
251 highlights a lipogenic pathway regulated by neuronal LPL loss. This is consistent with previous
252 studies in which liver lipids were altered following differential metabolic sensing in the brain.
253 Specifically, central administration of glucose has been shown to mimic the 'fed state' in the brain
254 and lower hepatic *SCD1* activity leading to reduced MUFA synthesis [6].
255
256   Preautonomic neurons in the PVN are known to contribute to the ANS regulation of hepatic
257 metabolism [32]. Here, we identified liver-related PVN neurons and determined their synaptic
258 regulation in mice lacking neuronal LPL. Our data clearly showed reduced sIPSCs in liver-related
259 PVN neurons in LPL KD mice (P<0.05 vs. WT) (Fig. 3C), suggesting that the inhibitory synaptic
260 regulation of liver-related PVN neurons in these mice is altered. Although further studies are needed
261 to elucidate the mode of neurotransmission, studies have highlighted the role of GABAergic
262 inhibition in the regulation of preautonomic neurons. For example, blockade of GABA$_A$ receptors in
263 the PVN caused a pronounced increase in plasma glucose concentration via sympathetic nerves to
264 the liver [20]. This suggests that reduced inhibition of sympathetic PVN neurons may be detrimental
265 to glucose homeostasis. However, at this stage, we cannot delineate whether neuronal LPL deficiency
266 results in decreased inhibition of pre-sympathetic or pre-parasympathetic neurons.
267
268   It is also plausible to suggest that the altered neuronal metabolism could result in changes to
269 synaptic function. To monitor changes in neuronal metabolism *ex vivo*, we employed FLIM to
270 measure both NADH and FAD lifetime changes following LPL loss. Although an established method
271 for measuring endogenous metabolism [33, 34], this methodology has not previously been used to
272 further our understanding of neuronal metabolism. Here, we clearly show that free NADH is
273 increased in LPL deficient PVN neurons (Fig. 4D). Typically, this would suggest an increased flux
274 through glycolysis [35-37]. However, since neurons have a limited capacity to upregulate glycolysis
275 [38], increased glucose utilization through the PPP in neurons is more likely [21]. In further support
276 of this interpretation, we also observed a marked increase in fructose-1-6 bisphosphate in LPL-
277 deficient hypothalamic neurons (Fig. 5A). Due to the lack of 6-phosphofructo-2-kinase/fructose-2, 6-
278 bisphosphatase-3 ((Pfkfb3), fructose-6P, cannot be shuttled through traditional glycolytic routes, and
279 instead is converted to fructose-1-6 bisphosphate and shunted towards the PPP [39]. Therefore, an
280 accumulation of fructose-1-6 bisphosphate suggests an increase in glucose uptake, whether this also
281 suggests a block in the pathway preceding full oxidation of glucose, or recycling via gluconeogenesis

282 (unlikely in mammalian neurons) remains unclear. Interestingly, metabolite enrichment analysis
283 suggests that metabolites associated with the TCA and lactose metabolism are up-regulated in the
284 LPL KD cells (Supplemental figure 5-6). Since lactose synthesis predominantly occurs in the
285 mammary gland, these findings highlight a caveat in the non-cell type or tissue specific
286 MetaboAnalyst analysis, and are likely due to the enrichment in fructose-1-6 bisphosphate, which is
287 a key metabolite in several pathways of carbohydrate metabolism. The importance of glucose
288 transport in neurons has been demonstrated in several recent studies **[40]**, that challenge the well-
289 established astrocyte-neuron lactate shuttle (ANSL) hypothesis **[41]**, to suggest that glucose is the
290 major substrate for the typical, activated brain. Our data suggest that carbohydrate metabolism is
291 increased in LPL depleted neurons. Whether this altered substrate utilization is a compensatory
292 response to reduced lipid uptake following LPL loss is likely but remains to be determined.
293
294   FLIM analysis of endogenous neuronal metabolism in PVN neurons also revealed a marked
295 increase in free FAD (Fig. 4E). This suggests an increase in pathways in which free FAD would be
296 produced (e.g., complex II activity in the TCA **[42]**), and reduced 'flux' through pathways in which
297 FAD would be enzyme-bound (e.g., FA oxidation). This is supported by the increased TCA cycle
298 metabolites (citrate, malate, fumarate, and succinate) observed in the LPL KD N41 hypothalamic
299 neurons. This suggested partitioning is also consistent with increased glucose uptake and utilization,
300 driving the oxidative metabolism of glucose and/or its intermediary metabolites (i.e., lactate) during
301 reduced FA uptake and oxidation following LPL loss. Importantly, these data represent a single time-
302 point of analysis, and further studies including isotope tracer experiments are warranted to further
303 understand LPL-dependent changes in metabolic flux and neuronal substrate utilization.
304
305   Hypothalamic neurons, in specific sub-nuclei, sense the abundance of leptin, insulin,
306 neuropeptides, and FAs **[22, 43-45]**, which may result in ATP-dependent potassium channel
307 activation. Although neurons are thought to rely primarily on the oxidative metabolism of
308 glucose/lactate to fulfill bioenergetics needs, fatty acid oxidation may also be important for the
309 metabolism and function of hypothalamic neurons. For example, the inhibition of CPT-1 activity in
310 the hypothalamus results in reduced neuronal FA oxidation and increased accumulation of long-
311 chain fatty acids (LC-FAs) **[46]**. This shift in metabolism may signal a "fed state," resulting in marked
312 inhibition in food intake and reduced nutrient mobilization, i.e., EGP **[46]**. It is thought that the
313 accumulation of malonyl-CoA may play a key role in neuronal FA sensing since inhibition of fatty
314 acid synthase can suppress food intake in a malonyl-CoA dependent manner **[47]**. In addition,
315 malonyl-CoA is a potent inhibitor of CPT-1 and, thus, LC-FA oxidation. Here, we show that LPL-
316 depleted neurons in the PVN show increased free NADH and FAD, which is consistent with a
317 metabolic shift away from mitochondrial FA oxidation of LC-FAs (Fig 4D-E). In addition, we
318 demonstrate that neuronal cell lines lacking LPL have diminished accumulation of the LC-PUFAs,
319 whereas neuronal cell lines that overexpress LPL have increased accumulation of LC-PUFAs, such as
320 ETA, EPA, and DHA (Fig. 5C). Importantly, these data recapitulate our findings *in vivo*, showing
321 reduced LC-PUFA abundance in the brains of mice lacking neuronal LPL [11, 13], and highlight the
322 utility of this cell line for investigating underlying metabolic changes following LPL modulation.
323 Moreover, these data suggest that LPL is involved in neuronal uptake of LC-PUFAs, which may be
324 an important signal in the regulation of hepatic metabolism and nutrient mobilization. Findings from
325 existing literature would suggest that neuronal LC-PUFAs depletion may signal poor nutrient
326 availability to stimulate increased food intake and increased EGP **[46]**. While our data are in part
327 consistent with this notion, these studies have all been acute responses to modulated FA sensing and
328 do not take into account the potential for compensatory mechanisms that occur with aging. For
329 example, it is plausible that long-term changes in essential FA uptake have a larger impact over time
330 that the response to acute changes in nutrient availability. It is well-established LC-PUFAs are found
331 in either the C1 or C2 position of major phospholipid species that play critical roles in neuronal
332 functions such as growth, signaling, and excitatory and inhibitory synaptic transmission **[48]**.
333 Therefore, long-term reductions in LPL-mediated LC-PUFA uptake may have profound effects on

334 synaptic transmission and neuronal maintenance over time. Whether these translate to downstream
335 changes in systemic metabolism will be an important focus of future studies.
336

337 **4. Materials and Methods**

338 *4.1. Animals*

339   All animal procedures were performed in accordance with institutional regulations and the
340 institutional animal care and use ethics Committee at the University of Colorado Anschutz Medical
341 Campus. Male NEXCreLPLflox (LPL KD) and WT mice were generated as previously described and
342 housed in standard conditions. Since NEXCre(+/-);LPLflox, and NEXCre(-/-);LPLflox produced
343 similar phenotypes, these mice were grouped (LPL KD) for analysis. Mice were fed standard
344 laboratory chow diet until terminal experiments at 3 mo. (WT n= 4, LPL KD n=5), 6 mo. (WT n= 4,
345 LPL KD n= 8), 12 mo (WT n= 5, LPL KD n = 6), 18 mo. (WT n= 4, LPL KD n=7) (11). Mice were fasted
346 for four hours prior to tissue harvest. Body composition was measured on anesthetized mice by dual-
347 energy x-ray absorptiometry using a mouse densitometer (PIXImus2, Lunar Corp., Madison, WI).
348 The electrophysiological studies were conducted at Tulane University. The procedures were
349 approved by the Institutional Animal Care and Use Committee.
350

351 *4.2. Glucose and insulin tolerance tests*

352   Glucose and insulin tolerance tests were performed by bolus intraperitoneal injection of glucose
353 (1 g/kg) or insulin (0.75 units/kg), respectively. Blood glucose was measured from the tail using a
354 glucometer (OneTouch Ultra, Lifescan) at baseline (0) and 10, 20, 30, 45, 60, and 90 min after injection.
355

356 *4.3. Hyperinsulinemic-euglycemic clamps*

357   Before the clamp experiment, mice were fasted overnight. On the day of the clamp experiment,
358 mice were anesthetized, and an indwelling catheter was inserted in the right internal jugular vein
359 [49]. A three-way connector was attached to the catheter to deliver solutions intravenously. A 2-hour
360 hyperinsulinemic-euglycemic clamp was conducted in all four groups of mice with a primed (150
361 mU/kg body wt) and continuous infusion of insulin (Humulin; Eli Lilly, Indianapolis, IN) at a rate of
362 2.5, 5 or 10 mU/kg/min to raise plasma insulin within a physiological range. 20% glucose was infused
363 at variable rates to maintain glucose at basal concentrations. Blood samples (10 µl) were collected at
364 10 min intervals for measurement of plasma glucose concentration only. Basal and insulin-stimulated
365 whole-body glucose turnover was estimated with a continuous infusion of [3-^{3}H]glucose
366 (PerkinElmer, Boston, MA) for 2 h before the clamps (0.05 µCi/min) and throughout the clamps (0.1
367 µCi/min), respectively. To estimate insulin-stimulated glucose uptake in individual organs, 2-deoxy-
368 D-[1- ^{14}C] glucose (2-[^{14}C]-DG) was administered as a bolus (10 µCi) when euglycemic clamp has
369 approached. 10 min after 2-[^{14}C]-DG being injected, tissues were taken for biochemical analysis.
370

371 *4.4. Analysis of liver lipids*

372   Neutral lipid was analyzed as described previously [50-52]. Frozen liver tissue was
373 homogenized in (v/v) Folch reagent (2:1 CHCl3/MeOH) containing 300 µg of tritridecanoin reference
374 standard (Nu-Check Prep Inc., Elysian, MN) by bead homogenization for two cycles of 2 min at 30
375 Hz. Homogenates were diluted further with Folch reagent to 4 ml, treated with 800 µl of 0.9% sodium
376 chloride solution, vortexed, and centrifuged at 4000 rpm for 5 min. The organic phase was removed
377 and dried under N2 gas. Total lipids were resuspended in 330 µl of 100% chloroform and applied to
378 HyperSep SI SPE columns (Thermo Scientific, Waltham, MA) pre-equilibrated with 15 column
379 volumes chloroform. Neutral lipids were eluted with a total of 3 ml of chloroform, dried under N2,

380   and resuspended in 1 ml of methanol containing 2.5% H2 SO4. Fatty acid methyl ester (FAME)
381   production was initiated by heating at 80 °C for 1.5 h. 1 ml of HPLC-grade water was added to quench
382   the reactions, and FAMEs/cholesterol was extracted with 200 μl of hexane. A Trace 1310 gas
383   chromotograph with a TG-5MS column (Thermo Scientific, Waltham, MA) was used to separate
384   lipids chromatographically, Lipids were detected with an ISQ single quadrupole mass spectrometer
385   (Thermo Scientific, Waltham, MA) in electron ionization mode. Masses were scanned between 40
386   amu and 550 amu with a scan time of 0.25 seconds, and temperatures were ramped from 50°C to
387   290°C in 3 stages.   Xcalibur software (Thermo Scientific) was used to calculate peak areas. Areas
388   were normalized to the tritridecanoin reference standard and then to tissue weight. Histological
389   analysis and scoring of hepatic lipids and steatosis were performed as previously described **[53]**.
390

391   *4.5. Lipoprotein Profile*

392   Plasma samples (200 μL) were chromatographed via fast protein liquid chromatography (FPLC)
393   using two Superose 6 columns in series as previously reported **[54]**. During size exclusion, the
394   absorbance of the eluted samples was measured at 280 nm allowing identification of each lipoprotein
395   class via protein content. Fractions containing either VLDL, LDL or HDL, were pooled, and
396   cholesterol was measured using a commercially available kit (Cayman Chemical Company, Ann
397   Arbor, MI, USA) following procedures outlined in the package insert.

398

399   *4.6. Quantitative real-time PCR*

400   Total RNA was reverse transcribed with the iScript cDNA synthesis kit (Bio-Rad, Hercules, CA).
401   Quantitative PCR was performed using primer sets for genes of interest and reference genes
402   (designed using NCBI's Primer3/BLAST) and iTaq Universal SYBR Green Supermix (Bio-Rad)
403   following the manufacturer's protocols. Reactions were run in duplicate on an iQ5 Real-Time PCR
404   detection system (Bio-Rad) along with a no-template control per gene. Validation experiments were
405   performed to demonstrate that efficiencies of target and reference genes were approximately equal.
406   Data were normalized to two reference genes (GAPDH and ACTB) using the comparative Ct method.
407

408   *4.7. Identification of liver-related neurons with PRV-152*

409   Retrogradely transported pseudorabies viral vector (PRV-152, provided by the Center for
410   Neuroanatomy with Neurotropic Viruses) expressing enhanced green fluorescent protein (EGFP)
411   was used to identify liver-related neurons **[17, 55, 56]**. Under anesthesia, the liver was exposed with
412   a small transverse incision, and ~4 μl of PRV-152 was injected into the median lobe of the liver (2
413   injections of 2 sites). A drop of adhesive "liquid bandage" was used to seal each injection to prevent
414   the leakage of the virus. The animals were maintained in a biosafety level 2 facility up to 110 h post-
415   injection.
416

417   *4.8. Brain slice preparation*

418   Acute brain slices were prepared from WT and LPL KD mice. After anesthesia with isoflurane,
419   the brain was removed and immersed in ice-cold oxygenated artificial cerebrospinal fluid (aCSF)
420   containing the following (in mM): 124 NaCl, 26 NaHCO$_3$, 1.4 NaH$_2$PO$_4$, 11 glucose, 3 KCl, 1.3 MgCl$_2$,
421   1.5 CaCl$_2$, pH 7.3-7.4. Transverse hypothalamic slices containing the PVN (300μm) were made using
422   a vibrating microtome. The slices were stored in a holding chamber at 34-36°C, and then transferred
423   to a recording chamber mounted on a fixed stage under an upright microscope (Nikon FN1).
424

425   *4.9. Whole-cell patch-clamp recordings*

426   Whole-cell patch-clamp recordings were performed at 34-36 ˚C from liver-related neurons in
427   the PVN identified under 40x water-immersion objective (N.A=0.8). Epifluorescence was used to
428   identify EGFP-containing neurons and infrared illumination and differential interference contrast
429   optics (IR-DIC) to target specific cells. For whole-cell patch-clamp recordings, electrodes (3-7 MΩ)
430   were filled with a solution containing the following (in mM): 130 Cs+ gluconate, 10 HEPES, 5 EGTA,
431   1 NaCl, 1 MgCl2, 1 CaCl2, 3 CsOH , 2-3 Mg-ATP, 0.2% biocytin, pH 7.3-7.4. Electrophysiological
432   signals were recorded using an Axoclamp 700B amplifier (Molecular Devices) and acquired by
433   pClamp (Molecular Devices). Inhibitory post-synaptic currents (IPSCs) were recorded at -10 mV and
434   excitatory post-synaptic currents (EPSCs) at -60 mV. Data were analyzed offline using pClamp or
435   MiniAnalysis (Synaptosoft).
436

437   *4.10. Stereotaxic AVV injection*

438   Adeno-associated virus 8 coding for Cre recombinase and GFP under the control of the CaMKIIa
439   promoter (AAV8-CaMKIIa-GFP-Cre, UNC viral core) was utilized to achieve recombination between
440   flox sites of PVN neurons. Adeno-associated virus 8 coding for GFP under the control of the CaMKIIa
441   promoter (AAV8-CaMKII-GFP, UNC viral core) was used as a control vector (mice referred to as
442   PVN nLPL+). 10-week old male LPL flox/flox mice were anesthetized with 2.0% isoflurane, and the
443   surgical anesthesia plane was maintained with 1.0% isoflurane. The incision site was locally
444   anesthetized with 100-200 μl of lidocaine (1 mg/mL). Mice were then mounted onto the stereotaxic
445   apparatus (Neurostar). 100 nL of the virus was injected bilaterally into the PVN (anteroposterior −0.7
446   mm, lateral +/- 0.25 mm, and dorsoventral −4.8 mm) using 0.5 μl Hamilton syringe (part# 86250,
447   Hamilton Company) at a rate of 20 nL/min **[57]**. The syringe was kept in place for 5 minutes after
448   each infusion, and the needle was withdrawn over 3 minutes. Two weeks following the initial
449   injection, anesthetized mice were transcardially perfused with HBSS (with calcium and Magnesium),
450   and whole brains were fresh-frozen in liquid nitrogen-cooled 2-methylbutane, since fixed brains are
451   incompatible with Fluorescence Lifetime Imaging Microscopy.

452   *4.11. Fluorescence Lifetime Imaging Microscopy (FLIM)*

453   FLIM was performed to detect local metabolic changes in 5-7 different areas of PVN in fresh
454   brain sections using a Zeiss 780 laser-scanning confocal/multiphoton-excitation fluorescence
455   microscope with a 34-Channel GaAsP QUASAR Detection Unit and non-descanned detectors for 2-
456   photon fluorescence (Zeiss, Thornwood, NY) equipped with an ISS A320 FastFLIM box and a
457   titanium:sapphire Chameleon Ultra II (Coherent, Santa Clara, CA). The 2-photon excitation was
458   blocked by a 2-photon emission filter. For the acquisition of FLIM images, fluorescence for
459   Nicotinamide Adenine Dinucleotide (NADH) and Flavin Adenine Dinucleotide (FAD) was detected
460   simultaneously by two photon-counting PMT detectors (H7422p-40; Hamamatsu). Images of the
461   different areas of PVN in the brains were obtained with Vista Vision software by ISS in 256x256
462   format with a pixel dwell time of 6.3 μs/pixel and averaging over 30 frames. Calibration of the system
463   was performed by measuring the known lifetime of the fluorophore fluorescein with a single
464   exponential decay of 4.0 ns **[58]**. The phasor transformation and data analysis were carried out using
465   Global SimFCS software (Laboratory for Fluorescence Dynamics (LFD), University of California,
466   Irvine) as described previously **[59]**. The number of pixels covered with lifetimes for the free and
467   bound reduced form of NADH and FAD were calculated in SimFCS (LFD), and the values were
468   normalized to the total number of pixels detected as previously described **[60, 61]**.
469   The glycolytic index was calculated for all experimental groups using the following equation:
470

471
$$\frac{free\ NADH\ fraction}{bound\ to\ enzyme\ NADH\ fraction}$$

472
473   as defined previously **[42, 61]**.
474

475   *4.12. Cell Culture conditions and Reagents*

476   mHypoE41 (N41) immortalized mouse hypothalamic neurons were purchased from
477   CELLutions Biosystems (Winnipeg, MB). N41 cells were grown in DMEM containing 1000 mg/L
478   glucose and 10% FBS at 37°C in the presence of 5% CO_2. To produce cells for stable overexpression
479   of LPL (N41 OE) or empty vector (control), N41 cells were transduced with MSCV as previously
480   described [10]. To produce stable knockdown cells, N41 cells were transduced with shRNA (N41 553
481   [LPL KD]), or scrambled RNA (N41 202 [control]), containing lentivirus, as previously described [10].

482   *4.13. Metabolomics*

483   Hypothalamic cell lines described above, were grown to 85% confluence. Each cell line was analyzed
484   in triplicate. Frozen cell pellets were extracted at 2e6 cells/mL in ice-cold lysis/extraction buffer
485   (methanol:acetonitrile:water 5:3:2 v/v/v). Ultra HPLC (UHPLC)-MS-based high throughput
486   metabolomics was performed at the University of Colorado School of Medicine Metabolomics Core.
487   Metabolites were separated using a 9-minute C18-based gradient method as previously described
488   [62], using a Thermo Vanquish UHPLC coupled to a Thermo Q Exactive mass spectrometer. In brief,
489   extracts (10 µl) were resolved in a Kinetex C18 column using a 3-minute isocratic gradient at 250
490   µl/minute (mobile phase: 5% acetonitrile, 95% 18 MOhm H_2O, 0.1% formic acid) or a 9-minute
491   gradient (5% B for the first 2 minutes, 5%–95% B over 1 minute, hold at 95% for 2 minutes, 95%–5%
492   B over 1 minute, re-equilibrate for 3 minutes). Quality control was performed via the assessment of a
493   technical mix injected after every 10 samples, as well as by comparison of internal standards.
494   Metabolite assignments were performed with the software MAVEN [63], upon conversion of .raw
495   files into the .mzXML format using MassMatrix (www.massmatrix.net). Assignments were further
496   confirmed by chemical formula determination from isotopic patterns, accurate intact mass, and
497   retention time comparison against an in-house standard library (Sigma-Aldrich, IROATech).
498   Pathway analysis and analysis of metabolite set enrichment was performed using MetaboAnalyst
499   using the positively regulated metabolites for either the LPL OE or LPL KD lines, normalized to the
500   respective controls [64, 65].

501   *4.14. Statistical analysis*

502   For electrophysiological experiments, continuous recordings have been conducted, and 2-
503   minute periods were analyzed with MiniAnalysis (Synaptosoft) to measure peak amplitude and
504   frequency of post-synaptic currents. Comparison between groups was made with an unpaired two-
505   tailed Student's t-test. For all analyses, $P < 0.05$ was considered significant. Numbers are reported as
506   the mean, with standard error of the mean (SEM) unless otherwise described.
507   Two-way repeated measure ANOVA was performed for all age and time-related analyses, using
508   posthoc multiple comparisons with Bonferroni correction, using GraphPad 7 data analysis and
509   graphing software, with $P < 0.05$ being considered significant, and $P < 0.1$ a trend.
510   For metabolomics data, the values for each metabolite for either the LPL OE, or LPL KD N41
511   cells were normalized for their respective control line (empty vector or scrambled RNA). Differences
512   between the mean of LPL OE vs LPL KD were analyzed by students T-test with $P < 0.05$ being
513   considered significant.

514   **5. Conclusions**

515   The path to T2DM involves increased hepatic lipid accumulation, hepatic insulin resistance, and
516   increased EGP. Since the ANS can regulate hepatic metabolism, it offers a novel therapeutic target
517   for NAFLD and T2DM. However, mechanisms related to neuronal inputs to the ANS control of
518   hepatic metabolism remain unclear. Here, we have shown that mice with neuronal LPL deficiency
519   and obesity show improvements in glucose tolerance with aging. Moreover, these changes are
520   associated with reduced hepatic lipid content and altered synaptic activity of liver-related neurons
521   in the PVN of the hypothalamus. Loss of LPL has a marked effect on neuronal metabolism and can

shift substrate utilization towards glucose oxidation in the absence of LC-PUFA transport. Our findings suggest that neuronal LPL is a component of liver-related preautonomic neurons and highlight the modulation of neuronal lipid metabolism as an intervention strategy to preserve insulin sensitivity in the aged and obese.

Supplementary Materials: The supplementary materials can be found online https://zenodo.org/record/3967991#.XyOIWShKjb5

Author Contributions: K.D.B designed experiments, performed experiments, analyzed data, and wrote the paper. E. D., T.Y., S.G., A.E.L., H.G., performed experiments, analyzed data, and edited the paper. H.W., designed experiments, performed experiments, and analyzed data. A.Z., designed experiments, analyzed data, and wrote the paper. R.H.E designed experiments and edited the paper.

Conflicts of Interest: The authors declare no conflict of interest. The funders had no role in the design of the study; in the collection, analyses, or interpretation of data; in the writing of the manuscript, or in the decision to publish the results.

References

1.   Bril, F. and K. Cusi, *Management of Nonalcoholic Fatty Liver Disease in Patients With Type 2 Diabetes: A Call to Action.* Diabetes Care, 2017. **40**(3): p. 419-430.

2.   Fabbrini, E., S. Sullivan, and S. Klein, *Obesity and nonalcoholic fatty liver disease: biochemical, metabolic, and clinical implications.* Hepatology, 2010. **51**(2): p. 679-89.

3.   Perry, R.J., et al., *The role of hepatic lipids in hepatic insulin resistance and type 2 diabetes.* Nature, 2014. **510**(7503): p. 84-91.

4.   Yki-Jarvinen, H., *Non-alcoholic fatty liver disease as a cause and a consequence of metabolic syndrome.* Lancet Diabetes Endocrinol, 2014. **2**(11): p. 901-10.

5.   Ribeiro, I.M.R. and V.R. Antunes, *The role of insulin at brain-liver axis in the control of glucose production.* Am J Physiol Gastrointest Liver Physiol, 2018. **315**(4): p. G538-G543.

6.   Lam, T.K., et al., *Brain glucose metabolism controls the hepatic secretion of triglyceride-rich lipoproteins.* Nat Med, 2007. **13**(2): p. 171-80.

7.   Yue, J.T., et al., *A fatty acid-dependent hypothalamic-DVC neurocircuitry that regulates hepatic secretion of triglyceride-rich lipoproteins.* Nat Commun, 2015. **6**: p. 5970.

8.   Song, B.J., et al., *Genetic ablation of CD36 does not alter mouse brain polyunsaturated fatty acid concentrations.* Lipids, 2010. **45**(4): p. 291-9.

9.   Laperrousaz, E., et al., *Lipoprotein lipase in hypothalamus is a key regulator of body weight gain and glucose homeostasis in mice.* Diabetologia, 2017. **60**(7): p. 1314-1324.

10.   Libby, A.E., et al., *Lipoprotein lipase is an important modulator of lipid uptake and storage in hypothalamic neurons.* Biochem Biophys Res Commun, 2015. **465**(2): p. 287-92.

11.   Wang, H., et al., *Deficiency of lipoprotein lipase in neurons modifies the regulation of energy balance and leads to obesity.* Cell Metab, 2011. **13**(1): p. 105-13.

12.   Wang, H., et al., *Obesity development in neuron-specific lipoprotein lipase deficient mice is not responsive to increased dietary fat content or change in fat composition.* Metabolism, 2016. **65**(7): p. 987-97.

564 13. Yu, T., et al., *Deficiency of Lipoprotein Lipase in Neurons Decreases AMPA Receptor Phosphorylation and Leads*
565   *to Neurobehavioral Abnormalities in Mice.* PLoS One, 2015. **10**(8): p. e0135113.

566 14. Ayala, J.E., et al., *Considerations in the design of hyperinsulinemic-euglycemic clamps in the conscious mouse.*
567   Diabetes, 2006. **55**(2): p. 390-7.

568 15. Jelenik, T., et al., *Mechanisms of Insulin Resistance in Primary and Secondary Nonalcoholic Fatty Liver.*
569   Diabetes, 2017. **66**(8): p. 2241-2253.

570 16. Kawano, Y. and D.E. Cohen, *Mechanisms of hepatic triglyceride accumulation in non-alcoholic fatty liver*
571   *disease.* J Gastroenterol, 2013. **48**(4): p. 434-41.

572 17. Gao, H., et al., *Transient receptor potential vanilloid type 1-dependent regulation of liver-related neurons in the*
573   *paraventricular nucleus of the hypothalamus diminished in the type 1 diabetic mouse.* Diabetes, 2012. **61**(6): p.
574   1381-90.

575 18. Gunion, M.W., et al., *Bombesin microinfusion into the rat hypothalamic paraventricular nucleus increases blood*
576   *glucose, free fatty acids and corticosterone.* Brain Res, 1989. **478**(1): p. 47-58.

577 19. Ionescu, E., et al., *Paraventricular nucleus modulation of glycemia and insulinemia in freely moving lean rats.*
578   Am J Physiol, 1989. **257**(6 Pt 2): p. R1370-6.

579 20. Kalsbeek, A., et al., *Suprachiasmatic GABAergic inputs to the paraventricular nucleus control plasma glucose*
580   *concentrations in the rat via sympathetic innervation of the liver.* J Neurosci, 2004. **24**(35): p. 7604-13.

581 21. Magistretti, P.J. and I. Allaman, *A cellular perspective on brain energy metabolism and functional imaging.*
582   Neuron, 2015. **86**(4): p. 883-901.

583 22. Bruinstroop, E., et al., *Hypothalamic neuropeptide Y (NPY) controls hepatic VLDL-triglyceride secretion in*
584   *rats via the sympathetic nervous system.* Diabetes, 2012. **61**(5): p. 1043-50.

585 23. Cheng, L., et al., *Palmitic acid induces central leptin resistance and impairs hepatic glucose and lipid metabolism*
586   *in male mice.* J Nutr Biochem, 2015. **26**(5): p. 541-8.

587 24. Obici, S., et al., *Decreasing hypothalamic insulin receptors causes hyperphagia and insulin resistance in rats.*
588   Nat Neurosci, 2002. **5**(6): p. 566-72.

589 25. Denis, G.V. and J.A. Hamilton, *Healthy obese persons: how can they be identified and do metabolic profiles*
590   *stratify risk?* Curr Opin Endocrinol Diabetes Obes, 2013. **20**(5): p. 369-76.

591 26. Bluher, M., *The distinction of metabolically 'healthy' from 'unhealthy' obese individuals.* Curr Opin Lipidol,
592   2010. **21**(1): p. 38-43.

593 27. Samocha-Bonet, D., et al., *Insulin-sensitive obesity in humans - a 'favorable fat' phenotype?* Trends
594   Endocrinol Metab, 2012. **23**(3): p. 116-24.

595 28. Shimazu, T., *Glycogen synthetase activity in liver: regulation by the autonomic nerves.* Science, 1967.
596   **156**(3779): p. 1256-7.

597 29. Shimazu, T., *Regulation of glycogen metabolism in liver by the autonomic nervous system. V. Activation of*
598   *glycogen synthetase by vagal stimulation.* Biochim Biophys Acta, 1971. **252**(1): p. 28-38.

599 30. Sigala, B., et al., *Sympathetic nervous system catecholamines and neuropeptide Y neurotransmitters are*
600   *upregulated in human NAFLD and modulate the fibrogenic function of hepatic stellate cells.* PLoS One, 2013.
601   **8**(9): p. e72928.

602 31. Hurr, C., et al., *Liver sympathetic denervation reverses obesity-induced hepatic steatosis.* J Physiol, 2019.

603 32. O'Hare, J.D. and A. Zsombok, *Brain-liver connections: role of the preautonomic PVN neurons.* Am J Physiol
604   Endocrinol Metab, 2016. **310**(3): p. E183-9.

605 33. Friedman, J.E., et al., *Pyrroloquinoline quinone prevents developmental programming of microbial dysbiosis*
606   *and macrophage polarization to attenuate liver fibrosis in offspring of obese mice.* Hepatol Commun, 2018. **2**(3):
607   p. 313-328.

608 34. Ranjit, S., et al., *Measuring the effect of a Western diet on liver tissue architecture by FLIM autofluorescence*
609   *and harmonic generation microscopy.* Biomed Opt Express, 2017. **8**(7): p. 3143-3154.

610 35. Stringari, C., et al., *Phasor fluorescence lifetime microscopy of free and protein-bound NADH reveals neural*
611   *stem cell differentiation potential.* PLoS One, 2012. **7**(11): p. e48014.

612 36. Drozdowicz-Tomsia, K., et al., *Multiphoton fluorescence lifetime imaging microscopy reveals free-to-bound*
613   *NADH ratio changes associated with metabolic inhibition.* J Biomed Opt, 2014. **19**(8): p. 086016.

614 37. Ranjit, S., et al., *Determination of the metabolic index using the fluorescence lifetime of free and bound NADH*
615   *in the phasor approach.* J Biophotonics, 2019: p. e201900156.

616 38. Bolanos, J.P., A. Almeida, and S. Moncada, *Glycolysis: a bioenergetic or a survival pathway?* Trends
617   Biochem Sci, 2010. **35**(3): p. 145-9.

618 39. Herrero-Mendez, A., et al., *The bioenergetic and antioxidant status of neurons is controlled by continuous*
619   *degradation of a key glycolytic enzyme by APC/C-Cdh1.* Nat Cell Biol, 2009. **11**(6): p. 747-52.

620 40. Dienel, G.A., *Brain lactate metabolism: the discoveries and the controversies.* J Cereb Blood Flow Metab, 2012.
621   **32**(7): p. 1107-38.

622 41. Pellerin, L. and P.J. Magistretti, *Glutamate uptake into astrocytes stimulates aerobic glycolysis: a mechanism*
623   *coupling neuronal activity to glucose utilization.* Proc Natl Acad Sci U S A, 1994. **91**(22): p. 10625-9.

624 42. Wallrabe, H., et al., *Segmented cell analyses to measure redox states of autofluorescent NAD(P)H, FAD & Trp*
625   *in cancer cells by FLIM.* Sci Rep, 2018. **8**(1): p. 79.

626 43. Broberger, C., et al., *Neuropeptide Y innervation and neuropeptide-Y-Y1-receptor-expressing neurons in the*
627   *paraventricular hypothalamic nucleus of the mouse.* Neuroendocrinology, 1999. **70**(5): p. 295-305.

628 44. Pocai, A., et al., *Hypothalamic K(ATP) channels control hepatic glucose production.* Nature, 2005. **434**(7036):
629   p. 1026-31.

630 45. van den Hoek, A.M., et al., *Intracerebroventricular administration of neuropeptide Y induces hepatic insulin*
631   *resistance via sympathetic innervation.* Diabetes, 2008. **57**(9): p. 2304-10.

632 46. Obici, S., et al., *Inhibition of hypothalamic carnitine palmitoyltransferase-1 decreases food intake and glucose*
633   *production.* Nat Med, 2003. **9**(6): p. 756-61.

634 47. Loftus, T.M., et al., *Reduced food intake and body weight in mice treated with fatty acid synthase inhibitors.*
635   Science, 2000. **288**(5475): p. 2379-81.

636 48. Bazan, N.G., *Synaptic lipid signaling: significance of polyunsaturated fatty acids and platelet-activating factor.*
637   J Lipid Res, 2003. **44**(12): p. 2221-33.

638 49. Kim, H.J., et al., *Differential effects of interleukin-6 and -10 on skeletal muscle and liver insulin action in vivo.*
639   Diabetes, 2004. **53**(4): p. 1060-7.

640 50. Libby, A.E., et al., *Perilipin-2 Deletion Impairs Hepatic Lipid Accumulation by Interfering with Sterol*
641   *Regulatory Element-binding Protein (SREBP) Activation and Altering the Hepatic Lipidome.* J Biol Chem,
642   2016. **291**(46): p. 24231-24246.

643 51. Orlicky, D.J., et al., *Perilipin-2 promotes obesity and progressive fatty liver disease in mice through*
644   *mechanistically distinct hepatocyte and extra-hepatocyte actions.* J Physiol, 2019. **597**(6): p. 1565-1584.

645 52. Libby, A.E., et al., *Perilipin-2 deletion promotes carbohydrate-mediated browning of white adipose tissue at*
646   *ambient temperature.* J Lipid Res, 2018. **59**(8): p. 1482-1500.

647 53. Bruce, K.D., et al., *Maternal high-fat feeding primes steatohepatitis in adult mice offspring, involving*
648   *mitochondrial dysfunction and altered lipogenesis gene expression.* Hepatology, 2009. **50**(6): p. 1796-808.

649 54. Jenkins, A.J., et al., *Serum lipoproteins in the diabetes control and complications trial/epidemiology of diabetes*
650   *intervention and complications cohort: associations with gender and glycemia.* Diabetes Care, 2003. **26**(3): p.
651   810-8.

652 55. Gao, H., et al., *Overactivity of Liver-Related Neurons in the Paraventricular Nucleus of the Hypothalamus:*
653   *Electrophysiological Findings in db/db Mice.* J Neurosci, 2017. **37**(46): p. 11140-11150.

654 56. Zsombok, A., et al., *Immunohistochemical localization of transient receptor potential vanilloid type 1 and*
655   *insulin receptor substrate 2 and their co-localization with liver-related neurons in the hypothalamus and*
656   *brainstem.* Brain Res, 2011. **1398**: p. 30-9.

657 57. Krashes, M.J., et al., *An excitatory paraventricular nucleus to AgRP neuron circuit that drives hunger.* Nature,
658   2014. **507**(7491): p. 238-42.

659 58. Berezin, M.Y. and S. Achilefu, *Fluorescence lifetime measurements and biological imaging.* Chem Rev, 2010.
660   **110**(5): p. 2641-84.

661 59. Digman, M.A., et al., *The phasor approach to fluorescence lifetime imaging analysis.* Biophys J, 2008. **94**(2): p.
662   L14-6.

663 60. Marwan, A.I., et al., *Unique Heterogeneous Topological Pattern of the Metabolic Landscape in Rabbit Fetal*
664   *Lungs following Tracheal Occlusion.* Fetal Diagn Ther, 2018.

665 61. Dobrinskikh, E., et al., *Heterogeneous Pulmonary Response After Tracheal Occlusion: Clues to Fetal Lung*
666   *Growth.* J Surg Res, 2019. **239**: p. 242-252.

667 62. McCurdy, C.E., et al., *Maternal obesity reduces oxidative capacity in fetal skeletal muscle of Japanese macaques.*
668   JCI Insight, 2016. **1**(16): p. e86612.

669 63. Melamud, E., L. Vastag, and J.D. Rabinowitz, *Metabolomic analysis and visualization engine for LC-MS*
670   *data.* Anal Chem, 2010. **82**(23): p. 9818-26.

671 64. Xia, J. and D.S. Wishart, *MSEA: a web-based tool to identify biologically meaningful patterns in quantitative*
672   *metabolomic data.* Nucleic Acids Res, 2010. **38**(Web Server issue): p. W71-7.

673 65. Xia, J. and D.S. Wishart, *MetPA: a web-based metabolomics tool for pathway analysis and visualization.*
674   Bioinformatics, 2010. **26**(18): p. 2342-4.

675

676